Computation of Heat Transfer with Solid/Liquid Phase Change Including Free Convection

G.E. Schneider*
University of Waterloo, Waterloo, Ontario, Canada

A computational model is presented for the prediction of solid/liquid phase-change energy transport including the influence of free convection. The computational model considers the velocity components of all nonliquid phase-change material control volumes to be zero but fully solves the coupled mass-momentum problem within the liquid. The thermal-energy model includes the entire domain and employs an enthalpy-like model in addition to recent developments for handling the phase-change interface nonlinearity. The predictions are compared with experimental data and with previous predictions for the test problem examined. The present procedure demonstrates both excellent agreement with the experimental data and a significant computational cost reduction from previous procedures.

Nomenclature

A	= finite difference coefficients
b	= right hand side
c	= specific heat
C	= transient coefficient
e	= specific energy
Fo	= Fourier modulus
g	= gravitational acceleration
h	= enthalpy
H	= half-height of domain
k	= thermal conductivity
n	= normal to interface
P	= pressure
Pr	= Prandtl number
Ra	= Rayleigh number
Ste	= Stefan number
T	= temperature
$u,v,$	= Cartesian velocity components
V_i	= interface velocity
W	= width of domain
x,y	= Cartesian coordinates
α	= thermal diffusivity
β	= isobaric compressibility
δ,Δ	= change in accompanying variable
γ	= nondimensional domain width
Γ	= modified diffusion coefficient
ϵ	= half-fusion temperature range
λ	= latent heat of fusion
ν	= kinematic viscosity
ρ	= density

Superscripts

c	= continuity
e,w,n,s,p	= geographical molecule location
u,v,p,T	= u and v velocity, pressure, temperature
$uu,up,vv,$ vp,TT	= equation of first variable, multiplier of second variable
(*)	= nondimensional

Subscripts

1,2,3	= solid, melt, or liquid
d	= dynamic
e	= east
f	= fusion
i,j	= discrete location
i	= interfacial or dummy variable
ℓ	= liquid
r	= reference
s	= solid
sp	= specified
w	= working variable
x,y	= x or y direction

Presented as Paper 85-0404 at the AIAA 23rd Aerospace Sciences Meeting, Reno, NV, Jan. 14-17, 1985; received March 5, 1985; revision received Jan. 7, 1986.

*Professor, Department of Mechanical Engineering. Member AIAA.

Introduction

PHASE-change energy storage systems involving the change of state from solid to liquid possess the capability of storing large quantities of thermal energy while experiencing relatively small temperature excursions at their exterior surfaces. As a result of this attribute, phase-change energy storage systems find application in the areas of solar energy storage systems, refrigerated cargo transport, spacecraft thermal control, and as a heat pipe variable conductance control mechanism. In order to assess the operational performance of such systems, however, it is necessary to determine the temperature time history of the system so that the impact of system surface temperature excursions on mating components can be evaluated.

The Stefan problem, describing energy transport within a phase-change material, is intrinsically highly nonlinear. This nonlinearity is due to the compatibility constraints imposed at the solidification/melt front and involves the energy fluxes and front propagation velocity at the interface location. However, neither the fluxes, the interface propagation velocity, nor the interface location itself are known a priori. As a result of this nonlinearity, analytical solutions to the Stefan problem are difficult, at best, and available for only a few relatively simple configurations.[1-5] For more realistic problem specifications, discrete methods are required to effect the solution. In this regard, the enthalpy finite difference model of Shamsundar and Sparrow is widely used.[6]

In the application of the enthalpy model to phase-change energy transport problems, the solution of the algebraic system of equations consumes a considerable amount of computing time. This is attributable to the complete transient histories that are generally required and, more significantly, to

the Gauss-Siedel iteration or an equivalent procedure that has been used to solve the equation system. The requirement for the use of an iterative solution method emerges from the highly nonlinear character of the interface compatability constraint.[7] In the enthalpy method, the interface location is not tracked explicitly and its precise location can be resolved only to within one mesh spacing. The interface compatibility constraint nonlinearity, however, appears in the enthalpy model in the form of a highly nonlinear equation of state relating enthalpy to temperature. In addition, this nonlinear behavior is highly concentrated within the immediate vicinity of the phase-change interface, and is extremely difficult to accommodate within the context of a simultaneous variable procedure for the equation system.[8] This difficulty is further augmented in problems for which more than one phase-change boundary must be accommodated within the domain.

Recently, Williams and Curry[9] presented a more implicit procedure for the solution of the algebraic equation system for the case of one-dimensional phase-change energy transport. In their paper, they attest to the difficulties involved in solving phase-change problems and provide a procedure for implementation to multiple interface problems. They achieve this through an energy distribution technique in the vicinity of phase-change interfaces which leads to a complex solution procedure. In addition, extension of their procedure to more than one space dimension does not appear to be possible.[10] Since the majority of problems of practical importance involve two or three space dimensions, this is a serious disadvantage of their procedure.

The numerical solution of solid/liquid phase-change problems has been considerably simplified and the associated costs dramatically reduced as a result of the method recently proposed by Schneider and Raw[11] for one-dimensional problems. This procedure has also been employed in a two-dimensional environment by Raw and Schneider[12] with comparable cost reductions to those observed for the one-dimensional situation. Cost reductions are typically two orders of magnitude.

All of the above-referenced methods and applications, however, have been restricted to conduction as the mode of energy transport without regard for buoyancy-induced free-convective motion. In practice, in terrestrial applications, it is frequently this free-convective motion itself which is the dominant mechanism for the thermal energy transport. As such, it is crucial that this fluid motion predictive capability be available in a computational scheme in order to predict energy transport with sufficient accuracy to be of practical value.

There has been relatively little work published to date in which the free-convective motion predictive capability is included in the numerical model. Recently, Gadgil and Gobin[13] and Ho and Viskanta[14] have presented models having this capability. However, both of these references quote extremely high computational times, which in itself is a prime reason for the scant treatment of this problem. Ho and Viskanta,[14] for example, quote run times of 50,000 CPU seconds for a single transient evolution using a CDC 6500 installation. This is clearly an exorbitant amount of computing time and is the reason that only two simulations were provided in their paper (a 13×21 grid was employed).

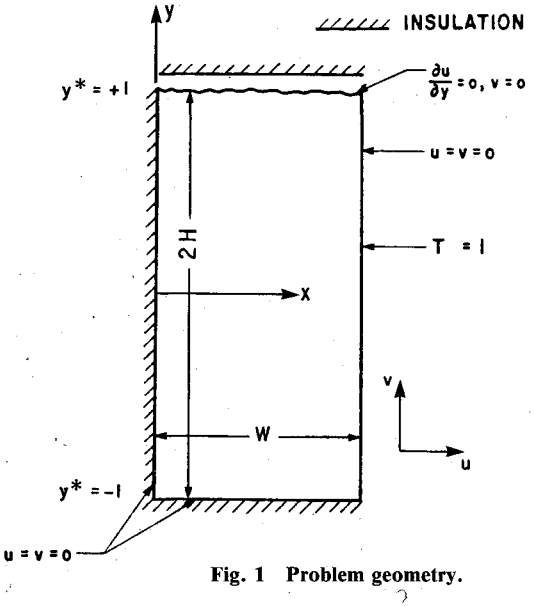

Fig. 1 Problem geometry.

In this paper, a procedure will be formulated which significantly reduces the computational costs of a phase-change model including free convection influences. The procedure employs an enthalpy-like model and incorporates the two rules proposed by Schneider and Raw.[11] Using the proposed model, in conjunction with a coupled, modified, strongly implicit procedure for the fluid flow solution, computational times for a complete transient simulation are reduced to less than 600 s for a 10×10 grid. This is a factor of 83 less than the 50,000 s quoted by Ho and Viskanta.[14] The author feels that this is an important step toward rendering the prediction of phase-change problems with free-convective motion practical for use as a design and analysis tool.

Mathematical Statement of the Problem

The problem examined in this work is that of thermal energy transport within a rectangular enclosure in which a phase-change material (PCM) is located and undergoes phase transition as its fusion temperature is traversed. The cavity has a height of $2H$ and a width of W. Schematically, the problem geometry is that shown in Fig. 1. A uniform temperature is applied at $x = W$ while the surfaces defined by $y = 0$ and $x = 0$ are insulated. These three surfaces are fixed and the PCM therefore has zero velocity at these surfaces. The remaining surface at $y = H$ is a free surface having an air layer between the upper surface of the PCM and the top, insulated surface of the container. This top surface has zero vertical velocity while the horizontal component of velocity has a zero vertical gradient imposed. The free surface is modeled as adiabatic due to the presence of the air layer. This problem configuration corresponds to that examined by Ho and Viskanta[14] for which limited experimental data are available.

The following nondimensional variables are introduced for this problem:

$$x^* \equiv x/H, \quad y^* \equiv y/H, \quad u^* \equiv u/u_0, \quad v^* \equiv v/u_0$$

$$\rho^* \equiv \frac{\rho}{\rho_\ell}, \quad \mu^* \equiv \frac{\mu}{\mu_\ell}, \quad k^* \equiv \frac{k}{k_\ell}, \quad P_d^* \equiv \frac{P_d}{P_0}$$

$$e^* \equiv \frac{e - e_r}{\Delta e_r}, \quad T^* \equiv \frac{T - T_r}{\Delta T_r}, \quad Fo \equiv \frac{t}{t_0} \tag{1}$$

In addition, the reference values are given by

$$u_0 \equiv \frac{\alpha_\ell}{H}, \quad P_0 \equiv \rho_\ell u_0^2, \quad t_0 \equiv \frac{L^2}{\alpha_\ell}$$

$$e_r \equiv e_f, \quad T_r \equiv T_f, \quad \Delta e_r \equiv c_\ell \Delta T_r \tag{2}$$

where $\Delta T_r = T_{sp} - T_f$ from boundary considerations. Furthermore, the pressure P is decomposed into two components as

$$P = P_d - \rho_0 g y \tag{3}$$

where y is vertical distance. Using the above definitions, the governing equations representing conservation of mass, momentum, and thermal energy can be written in nondimensional form as the following, considering incompressible liquid PCM and employing the Boussinesq approximation for

the buoyancy terms:

$$\frac{\partial}{\partial x^*}(u_\ell) + \frac{\partial}{\partial y^*}(v_\ell^*) = 0 \tag{4}$$

$$\frac{\partial}{\partial Fo}(u_\ell^*) + \frac{\partial}{\partial x^*}(u_\ell^* u_\ell^*) + \frac{\partial}{\partial y}(v_\ell^* u_\ell^*) = -\frac{\partial P_d^*}{\partial x^*} + Pr_\ell\left[\frac{\partial}{\partial x^*}\left(\frac{\partial u^*}{\partial x^*}\right) + \frac{\partial}{\partial y^*}\left(\frac{\partial u^*}{\partial y^*}\right)\right] - Pr_\ell Ra_\ell \frac{g_x}{g}(T^* - T_r^*) \tag{5}$$

$$\frac{\partial}{\partial Fo}(v_\ell^*) + \frac{\partial}{\partial x^*}(u_\ell^* v_\ell^*) + \frac{\partial}{\partial y^*}(v_\ell^* v_\ell^*) = -\frac{\partial P_d^*}{\partial y^*} + Pr_\ell\left[\frac{\partial}{\partial x^*}\left(\frac{\partial v^*}{\partial x^*}\right) + \frac{\partial}{\partial y^*}\left(\frac{\partial v^*}{\partial y^*}\right)\right] - Pr_\ell Ra_\ell \frac{g_y}{g}(T^* - T_r^*) \tag{6}$$

$$\frac{\partial}{\partial Fo}(e_\ell^*) + \frac{\partial}{\partial x^*}(u_\ell^* e_\ell^*) + \frac{\partial}{\partial y^*}(v_\ell^* e_\ell^*) = \frac{\partial}{\partial x^*}\left(\frac{\partial T^*}{\partial x^*}\right) + \frac{\partial}{\partial y^*}\left(\frac{\partial T^*}{\partial y^*}\right) \tag{7}$$

$$\frac{\partial}{\partial Fo}(\rho_s^* e_s^*) = \frac{\partial}{\partial x^*}\left(k_s^* \frac{\partial T_s^*}{\partial x^*}\right) + \frac{\partial}{\partial y^*}\left(k_s^* \frac{\partial T_s^*}{\partial y^*}\right) \tag{8}$$

In the above, the assumption has been that the velocity of the solid PCM is identically zero. The two parameters appearing in these equations are the Prandtl number and the Rayleigh number defined by

$$Pr_\ell \equiv \nu_\ell / \alpha_\ell$$

and

$$Ra_\ell \equiv \beta g H^3 \Delta T_r / \nu_\ell \alpha_\ell \tag{9}$$

where the subscript ℓ denotes evaluation based on liquid phase PCM. The differential equations [(4–7)] are the governing partial differential equations in nondimensional form. However, the choice for ΔT_r which appears in the definition of the Rayleigh number has not yet been justified. This is effected through consideration of boundary conditions. In addition to boundary conditions, however, the interfacial compatibility constraints must also be applied.

With regard to the interface compatibility constraints, continuity of temperature requires, in nondimensional form, that

$$T_\ell^*|_i = T_s^*|_i = T_f^* = 0 \tag{10}$$

Furthermore, to the continuity of temperature at the phase-change interface, conservation of energy must also be enforced across the interface. With reference to Fig. 2, conservation of energy applied to an interfacial surface element results in the nondimensional requirement that

$$-\frac{\partial T_\ell^*}{\partial n^*}\bigg|_i = -k_s^* \frac{\partial T_s^*}{\partial n^*}\bigg|_i + \frac{\rho_s^* V_i^*}{Ste} \tag{11}$$

In this constraint equation, n^* is a nondimensional coordinate perpendicular to the interface, V_i^* is the nondimensional interface propagation velocity, and the Stefan number, *Ste,* is defined as

$$Ste \equiv c_\ell \Delta T_r / \lambda \tag{12}$$

The boundary conditions required to complete the mathematical description of the problem are given as

$$x^* = 0; \quad u^* = 0, \quad v^* = 0, \quad \frac{\partial T^*}{\partial x^*} = 0 \tag{13}$$

$$y^* = -1; \quad u^* = 0, \quad v^* = 0, \quad \frac{\partial T^*}{\partial y^*} = 0 \tag{14}$$

$$y^* = +1; \quad \frac{\partial u}{\partial y^*} = 0, \quad v^* = 0, \quad \frac{\partial T^*}{\partial y^*} = 0 \tag{15}$$

$$x^* = \gamma, \quad u^* = 0, \quad v^* = 0, \quad T^* = 1 \tag{16}$$

where $\gamma \equiv W/H$ and where

$$\Delta T_r \equiv T_{sp} - T_f \tag{17}$$

has been introduced with T_{sp} being the specified value of temperature at the rightmost surface ($x^* = \gamma$).

With the exception of the equation of state, relating e^* to T^*, the problem specification is now complete. The equation of state will be introduced when the numerical procedure is discussed. However, for purposes of this paper the assumption will be further introduced that the property values of the PCM are independent of its phase. Thus

$$k_s^* \simeq c_s^* \simeq \rho_s^* \simeq 1 \tag{18}$$

The functional dependence of the temperature distribution then takes the form

$$T^* = T^*(x^*, y^*, Fo, \gamma, Pr, Gr, Ste) \tag{19}$$

where the subscript ℓ has now been dropped in view of the assumption of Eq. (18). The numerical solution procedure and the equation of state are presented in the following section.

Numerical Formulation

In this section the numerical procedure employed to solve the phase-change problem including free-convective motion is described. In order to include the free-convection influence on the thermal energy transport, of course, the fluid flow equations representing conservation of mass and momentum must be solved in addition to the thermal energy equation. Furthermore, the nonlinearity inherent in the interface compatibility constraints renders the energy equation extremely difficult to solve even for the case of pure diffusive transport. Thus the in-

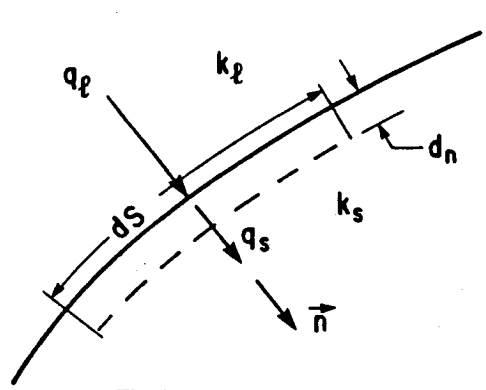

Fig. 2 Interface energy balance.

clusions of both the fluid flow motion and the phase-change nonlinearity leads to an extremely challenging problem indeed.

The finite difference method is used in the present work employing the staggered mesh commonly used for fluid-flow computation. This mesh is illustrated in Fig. 3 wherein three different control volumes are identified. Pressure and temperature variables are stored at the indicated "nodes," centered within mass and energy conservation control volumes, while the u and v velocity component variables are stored at the faces of these control volumes with momentum control volumes constructed around the respective velocity components as shown in the figure.

The discrete representation of the continuity equation is obtained by performing a mass balance on continuity control volumes. These control volumes are those having pressure nodes at the control volume centers. The discrete continuity equation for incompressible flow (see Fig. 3) has the form

$$A^{cu,e}u^*_{i,j} + A^{cu,w}u^*_{i-1,j} + A^{cv,n}v^*_{i,j} + A^{cv,s}v^*_{i,j-1} = 0 \qquad (20)$$

where the coefficients are the appropriate products of density and control volume surface areas. The discrete representation of the x-momentum equation is written in the form

$$A^{uu,w}u^*_{i-1,j} + A^{uu,s}u^*_{i,j-1} + A^{uu,p}u^*_{i,j} + A^{uu,e}u^*_{i+1,j} + A^{uu,n}u^*_{i,j+1} + A^{up,w}p^*_{i,j} + A^{up,e}P^*_{i+1,j} = b^u \qquad (21)$$

The coefficients in this equation are obtained using the procedure outlined by Patankar.[15] In particular, the momentum flows are evaluated using the power law approximation to the locally one-dimensional advection-diffusion problem. The central coefficient $A^{uu,p}$ is obtained from

$$A^{uu} = -(A^{uu,w} + A^{uu,s} + A^{uu,e} + A^{uu,n}) + C^u \qquad (22)$$

where

$$C^u = \rho^*(\delta x^*)_e \Delta y^*_j / \Delta Fo \qquad (23)$$

and where $(\delta x^*)_e$ is the x dimension of the momentum control volume. The source term of Eq. (21) includes the buoyancy driving force term and is given by

$$b^u = -Pr_\ell Ra_\ell \frac{g_x}{g}(T^*_{i,j} - T^*_r)(\delta x^*)_e \Delta y^*_j + C^u u^{*0}_{i,j} \qquad (24)$$

In a similar fashion, the discrete representation of the y-momentum equation can be determined. This equation has the form

$$A^{vv,w}v^*_{i-1,j} + A^{vv,s}v^*_{i,j-1} + A^{vv,p}v^*_{i,j} + A^{vv,e}v^*_{i+1,j} + A^{vv,n}v^*_{i,j-1} + A^{vp,s}P^*_{i,j} + A^{vp,n}P^*_{i,j+1} = b^v \qquad (25)$$

where

$$A^{vv,p} = -(A^{vv,w} + A^{vv,s} + A^{vv,e} + A^{vv,n}) + C^v \qquad (26)$$

with C^v given for this equation by

$$C^v = \rho^* \Delta x^*_i (\delta y^*)_n / \Delta Fo \qquad (27)$$

and with the source term given by

$$b^v = -Pr_\ell Ra_\ell (g_y/g)(T^*_{i,j} - T^*_r)\Delta x^*_i (\delta y^*)_n + C^v v^{*0}_{i,j} \qquad (28)$$

The thermal energy equation is treated somewhat analogously to the momentum equations. However, the thermal energy equation contains a mixture of internal energy terms and temperature terms, internal energy being stored and convected while temperature is the diffused variable. This mixture is resolved through the equation of state.

Following Schneider[11,12] the internal energy is approximated by the enthalpy of the substance and a piecewise linear equation of state is used to effect complete passage from solid, through "melt," to liquid. For this purpose, a phase transition, or melt phase, is introduced. Denoting the solid, phase transition, and liquid phases by the subscripts 1, 2, and 3, respectively, the equation of state is given by the single general equation

$$h^* = h^*_{r,i} + c^*_{p,i}(T^* - T^*_{r,t}), \qquad i = 1,2,3 \qquad (29)$$

where $c^*_{p,i}$ is normalized with respect to the liquid value and where the subscript r denotes a reference value. This reference value is chosen for convenience, since only changes in energy or enthalpy are required, but the constraint is required when dealing with the PCM that the equation of state must be continuous.

In nondimensional form, one consistent set of reference values is given by

$$\begin{aligned} h^*_{r,1} &= 0 & T^*_{r,1} &= -\epsilon & c^*_{p,1} &= c^*_s \\ h^*_{r,2} &= 0 & T^*_{r,2} &= -\epsilon & c^*_{p,2} &= 0.5/(Ste\cdot\epsilon) \\ h^*_{r,3} &= 1/Ste & T^*_{r,3} &= +\epsilon & c^*_{p,3} &= 1 \end{aligned} \qquad (30)$$

where ϵ is a small value, typically of order 10^{-4}, whose influence is equivalent to representation of the phase transition region by a very large specific heat over a negligibly small temperature range. In the discrete problem, therefore, the Stefan number appears through its appearance in the property relations whereas it appears in the continuum problem in the interface compatibility constraint.

The generalized equation of state can be rewritten in the more compact form

$$h^* = h^*_{w,i} + c^*_{p,i}T^* \qquad (31)$$

where h^* is defined analogously to e^* and where

$$h^*_{w,i} = h^*_{r,i} - c^*_{p,i}T^*_{r,i} \qquad (32)$$

The equation of state is illustrated graphically in Fig. 4.

Using the above form for the equation of state it is possible to express the energy equation in a form which is primarily

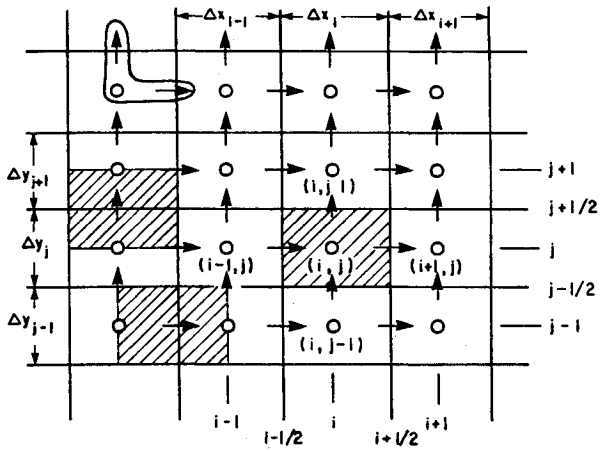

Fig. 3 Finite difference mesh.

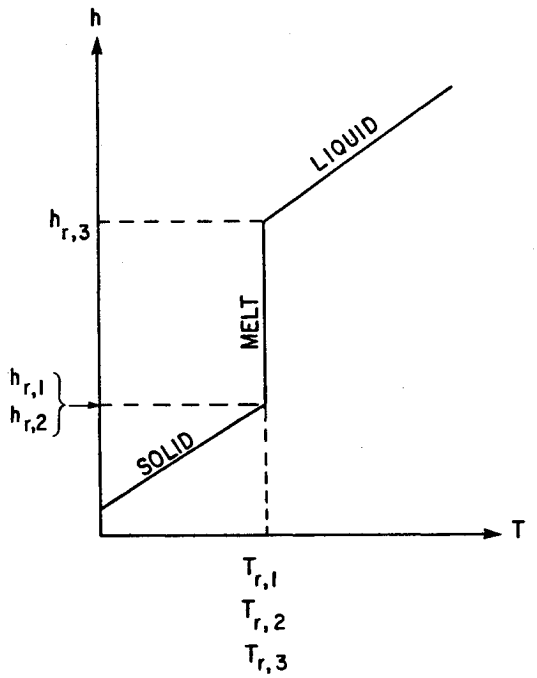

Fig. 4 Equation of state.

dependent on temperature. This equation has the form

$$A^{TT,w}T^*_{i-1,j}+A^{TT,s}T^*_{i,j-1}+A^{TT,p}T^*_{i,j}$$
$$+A^{TT,e}T^*_{i+1,j}+A^{TT,n}T^*_{i,j+1}=b^T \quad (33)$$

where

$$A^{TT,p}=-(A^{TT,w}+A^{TT,s}+A^{TT,e}+A^{TT,n})+C^Tc^*_{p,i}|_{i,j} \quad (34)$$

and where the evaluation of the A^{TT} terms, representing sensible energy flows, has been done using the methods of Patankar[15] where the effective coefficient for diffusion is given by

$$\Gamma^*=k^*/c^*_{p,i} \quad (35)$$

evaluated at the appropriate location. The power law approximation to the one-dimensional advection-diffusion problem must, of course, be multiplied by $c^*_{p,i}$ at the appropriate location to yield the correct sensible energy convection and pure diffusion in the corresponding limiting situations.The constant C in the above is given by

$$C^T\equiv\rho^*\Delta x^*_i\Delta y^*_j/\Delta Fo \quad (36)$$

and the right-hand side, B^T, is given by

$$b^T=C^Tc^*_{p,i}|_{i,j}T^{*0}_{i,j}-C^T(h^*_{w,i}-h^{*0}_{w,i})|_{i,j} \quad (37)$$

It is noted that the form of the equation given by Eq. (33), with Eqs. (35-37), involves relatively few occurrences of $h^*_{w,i}$ even though these values appear in every convective energy transport term of the energy balance. This is a result of the invocation, at discrete level, of the continuity equation. Each convection term leads to a mass flow times reference enthalpy contribution and it is further noted that the assumption, presented earlier, has been made that the velocity of nonliquid regions of the domain is identically zero. Thus, wherever a velocity component is in contact with a "melt" or solid control volume, that velocity will be zero. Therefore, the only nonzero velocity contributions to the energy equation are those corresponding to liquid flow, and since these flows have identical reference enthalpies their influence cancels exactly through conservation of mass. The net convection energy transport is then only the sensible component. However, the primary influence of convection, that of transporting highly energetic liquid to the phase-change interface, where it can contribute significantly to the phase-front erosion through melting, has been retained in the model.

The numerical problem has now been fully formulated, with boundary conditions treated in a straightforward manner. It remains to solve the strongly coupled and highly nonlinear equation system. The method of accomplishing this is discussed in the next section of the paper.

Numerical Solution Considerations

In phase-change energy transport, the entire problem is transient and temporally evolutionary, with all details of the transient evolution important to the problem resolution for use in design and analysis. Consequently, it is essential that sufficiently small time steps in this evolution be employed such that temporal accuracy is maintained. Such a temporal resolution renders the changes in the temperature field or in the fluid flowfield small from time step to succeeding time step and this significantly reduces, on a temporally local level, the nonlinear coupling between the energy and fluid flow equations. This realization is used to advantage in the present solution procedure to preclude energy-fluid flow equation iteration, and indeed to preclude the *nonlinear* iteration normally required of the fluid flow equations themselves. It is recognized, of course, that the justification for such a procedure presupposes implementation of a sufficiently small time step in the transient evolution. The remedy for inaccurate computations *from this source,* therefore, is to further decrease the time step. The algorithmic simplifications which result from such a procedure are significant, and fully justify its use.

The strategy for the transient evolution of the fluid flow and temperature fields, then, is that depicted by the following sequence of computations for advancement over a single time step:

1) Enter the new time-level computations with the velocity field and temperature distribution from the previous time step.

2) Using the above velocities and temperature field, coefficients are calculated for the fluid flow (i.e., mass and momentum) equation system.

3) The thereby linearized, but highly coupled, mass-momentum equation system is solved to yield the velocities and the pressure field for the new time level.

4) These new velocities are employed in the calculation of the coefficients for the discrete energy equation representation.

5) The thereby linearized (with new velocities) energy equation is solved to yield the predicted temperature distribution for the new time level.

6) As a result of steps 3 and 5, predictions at the new time level are available for the velocity field, the pressure field, and the temperature field. From this information, enthalpy and melt-fraction predictions can be determined directly.

7) The newly predicted values are assigned to the variable representing the previous time-step values, the time level is advanced, and the procedure is repeated from step 1 for the subsequent time level.

This procedure is noniterative in nature and requires that a fixed number of computational tasks be performed for each time step, each of which, by itself, is indeed a nontrivial task. In effect, of course, this procedure employs the time-evolutionary character of the problem as a nonlinear, coupling-feedback mechanism to accomplish a task equivalent to the normally required interequation interation. The list presents, in an algorithmic sequence, the overall computational strategy employed for each time step in the transient evolution. Some comments are necessary, however, to clarify certain of the individual tasks identified in this list.

The solution of the coupled mass-momentum equation system representing fluid flow is a significant task in the overall algorithm. The method employed for the coupled fluid-flow solution is the Coupled Modified Strongly Implicit Procedure of Schneider and Zedan.[16] In this procedure the extended Modified Strongly Implicit Procedure is used in conjunction with a derived equation for pressure (replacing the primitive form of the continuity equation for pressure) in a strongly implicit iteration algorithm. The derived equation for pressure renders the equation system more diagonally dominant than the original equation system and hence enhances the iterative convergence. It is noted, however, that this pressure equation is derived in such a manner that when the equation-system solution is obtained, the original continuity equation is indeed satisfied. While this solution procedure has slightly higher computational costs than do some other optimized procedures, the costs of these alternative procedures are relatively sensitive to the value of the (many) solution-procedure parameters and effecting the optimization frequently considerably exceeds the actual costs of solution. Conversely, the Coupled Modified Strongly Implicit Procedure has relatively few parameters with procedural performance more weakly dependent on the few procedure parameters. Thus, this procedure approaches that of a "black box" to which coefficients are provided and from which economical solutions are obtained.

With regard to the nonlinearity associated with the Stefan problem, an extension has been made of a procedure previously developed by the author for one-dimensional configurations.[12] This procedure has been extended to two dimensions and incorporated into the free-convective energy transport code. This procedure still requires iteration to resolve the nonlinearity. However, it is of a significantly different form, being closer to a predictor-corrector method than a point relaxation method. Each time step calculation proceeds as follows:

1) As a first guess, the phase distribution of a new $(n+1)$ time level is assumed to be the same as for the current (n) level.

2) On this assumption, the energy equation is assembled and solved directly (algebraic iteration is possible as well).

3) The new tentative temperature solution yields a new tentative phase distribution. The guessed and tentative phase distributions are compared, and by applying two rules, presented below, to the tentative phase distribution, a modified guess for the new phase distribution is generated.

4) Steps 2 and 3 are repeated until the modified and tentative phase distributions agree.

This step calculation procedure is simple but is contingent on two fundamental rules, which will be discussed shortly. Experience has shown that when the time interval is large enough to move the front by one control volume boundary per time step, typically only two or three iterations of steps 2 and 3 are required. If the conditions are such that the front doesn't cross a control volume boundary, then the first guess is correct and only one iteration is required. This has been shown to lead to a drastic reduction in execution cost.[11,12]

The two rules which enable this cost reduction follow directly from enforcing the correct physical behavior if the iterations are viewed as a transient evolution.

Rule 1. In a single iteration, the modified-guess phase for a particular-control volume can only change from its previous iteration value by one phase. Thus if the tentative phase is liquid and the guessed phase was solid, the modified guess will be restricted to the melt phase as a maximum excursion from its present state.

Rule 2. If the phase states of the previous iteration for a control volume and all its neighbors were the same, then the modified guess for the phase state of the control volume in question must remain unchanged. For example, if the tentative phase state of a control volume is liquid, but the previous guess for it and for all of its neighbors are solid, then the modified phase guess will remain the solid state.

The first of the above rules enforces the physical requirement that a phase change from solid to liquid, or vice versa, must pass through the melt phase. If this is not satisfied, the system will not have acknowledged the enthalpy difference that exists between the solid and liquid states. The second rule is a statement that enforces the physical requirement that a phase change in one region cannot occur without a neighboring region having changed phase first. This, of course, is restricted to zero internal source strength situations; but it can readily be modified to accommodate nonzero source strength conditions.

Subject to the assumed phase distribution, it is still required to obtain the solution of the energy equation algebraic system. If the correct phase distribution within the PCM is known, or a suitable temporarily fixed distribution is assumed as per the iteration sequence described earlier, the energy equation discretization represents a linear algebraic system, expressed in terms of the control volume temperatures, for which a solution is required. For small problem sizes, a direct solution procedure, equivalent to Gaussian elimination, may be employed. However, as the problem size grows the continued use of a direct solution procedure rapidly becomes prohibitively expensive and iterative methods *for the solution of the linearized problem* must be employed. The method selected for application to the energy transport equation is the Modified Strongly Implicit Procedure of Schneider and Zedan[17] incorporating the recommendations for enhanced convergence and stability of Schneider and Zedan.[18] This procedure has proven highly effective in the solution of field problems.

Comparison with Experiment

The computational model was executed for the problem of geometry of Fig. 1. This configuration corresponds to that examined experimentally and numerically by Ho and Viskanta,[14] although the numerical work of Ho and Viskanta was limited to a single computational run. The PCM is *n*-octadecane with a corresponding Prandtl number of $Pr_\ell = 50$. The Rayleigh number, based on the surface temperature-fusion temperature difference and on the half-height of the cell, is 1.57×10^7. The experiment was initiated with zero subcool, solid-phase conditions throughout and this was simulated in the numerical experiments with an initial nondimensional subcool of -0.002. The range of nondimensional temperature is from 0 to 1. The actual cavity dimensions of the Ho and Viskanta[14] experiment were 0.10 m total height and 0.05 m width. It is noted that the paper by Ho and Viskanta implies a cell height of 0.13 m but the actual height of 0.10 m is obtained from the thesis by Ho.[19]

On the basis of several test runs, it was determined that a nondimensional time step determined according to $Ste \cdot \Delta Fo = 10^{-4}$ provided accurate temporal resolution at early time. At later times, when the melt had more fully penetrated the PCM, this was gradually relaxed to $Ste \cdot \Delta Fo = 5 \times 10^{-3}$. Three different mesh discretizations were employed. These correspond to a 10×10 mesh (8×8 interior control volumes), a 20×20 mesh (18×18 interior control volumes), and a 40×20 mesh (38×18 interior control volumes). For the latter case, however, the 40×20 mesh was simulated using a 20×20 mesh on a domain of half the horizontal extent. The experimental data of Ho and Viskanta[14] extend only to a 25% melt fraction limit and the 20×20 grid, 40×20 simulation, fully captured this problem.

Qualitative results for this problem obtained from the 20×20 mesh are presented in Figs. 5 through 12 in terms of isotherms with superimposed velocity vector plots. In succession, these plots form the melting history profile for the problem. In all plots shown here the minimum and maximum isotherms correspond to values of 0 and 1, respectively, for nondimensional temperature. In Fig. 5, for $Fo = 0.2$, there is relatively little liquid-phase PCM and the fusion isotherm, $T^* = 0$ corresponding to the phase-front interface, is nearly

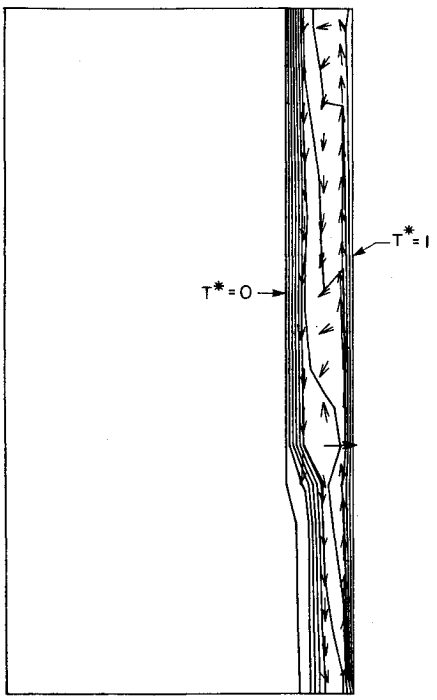

Fig. 5 Results for $Fo = 0.2$.

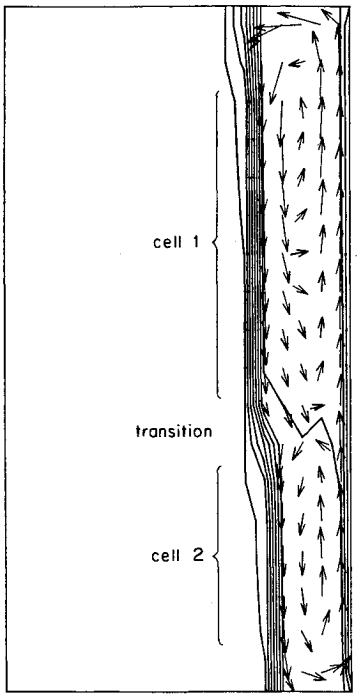

Fig. 6 Results for $Fo = 0.4$.

vertical. It is also clear from the figure that a large recirculation cell has been established within the liquid PCM. At $Fo = 0.4$, the liquid region has expanded while the interfacial front is still very nearly vertical. The strength of the recirculation has increased and it is also observed there are *two* recirculation cells beginning to emerge within a large overall recirculation cell. That is, part of the downward flow near the cold-phase front is "stripped off" and moves up while a similar phenomenon occurs at the hot wall. This occurs at approximately 40% distance from the bottom surface. However, this effect is relatively weak. It is noted that recirculation

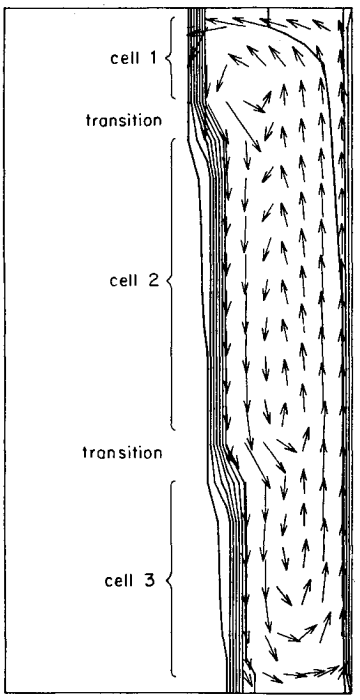

Fig. 7 Results for $Fo = 0.6$.

strength increases throughout the entire melt and that the velocity vectors are scaled to have a maximum length on the plots of 1 in. (2.54 cm). Thus the growth in convection strength is not exhibited from figure to figure in the sequence. Rather, the relative spatial convection strength within a specific plot is preserved.

Figure 7 corresponds to $Fo = 0.6$ and the weak secondary cells are also preserved in this figure. It is evident, however, that the recirculation in the top left region of the liquid is becoming considerably more vigorous as melting is proceeding. It is also evident that the interfacial front is beginning to depart more noticeably from its almost vertical configuration and that increased erosion of the melt front is occurring near the top of the PCM as is expected. Figure 8 corresponds to $Fo = 0.8$ and it is observed that the weak secondary recirculation zones are no longer present. The 0.6 isotherm displays strongly in this figure the "temperature inversion" phenomenon which occurs in strongly convecting buoyancy driven flows. The strong convection of warm fluid proceeds up along the heated wall, is deflected to the left and then down the phase-front interface side of the recirculation cell. Here the convective motion is of such a strength that the fluid does not cool to below the 0.6 level until it has almost reached the bottom surface once again. This is evidenced by the "finger-like" projections of the 0.6 isotherm in the central region of the liquid. Similarly there is a cold finger-like projection extending up the right side of the central liquid region.

In Fig. 9, corresponding to $Fo = 1.0$, the "stripping-off" effect is witnessed again quite strongly. In the top one-third of the liquid cavity there is a strong recirculation zone with the remaining surface flows continuing down the phase front to complete the primary circulation cycle. It is further noted that the effect of the vigorous cavity recirculation is to begin to isothermalize the central region of the liquid cavity. This influence is further observed in Figs. 10 to 12 wherein the central region of the liquid cavity is indeed nearly isothermal. In addition, it is observed in these figures that the interface front configuration continues to experience enhanced erosion of the top of the remaining PCM. In Figs. 9 to 11 there is a single primary recirculation with a continued "stripping off" of fluid, significantly through entrainment-like mechanisms, as

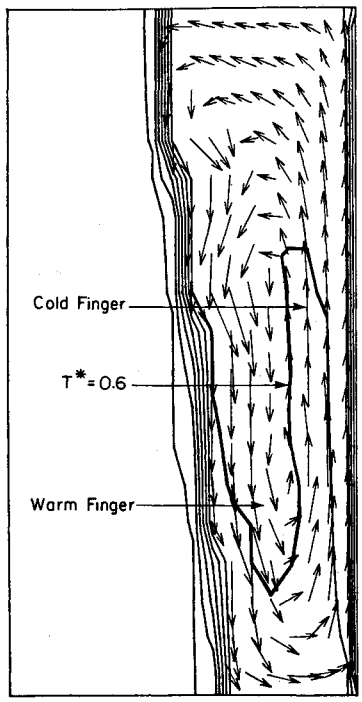

Fig. 8 Results for $Fo = 0.8$.

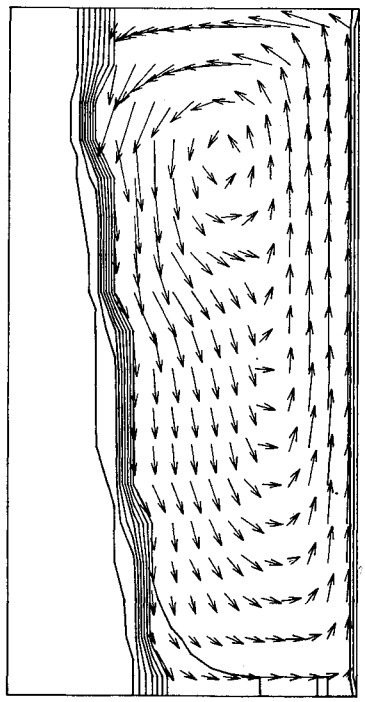

Fig. 10 Results for $Fo = 1.2$.

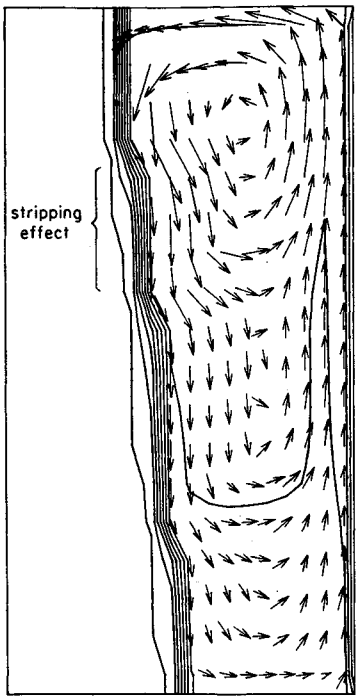

Fig. 9 Results for $Fo = 1.0$.

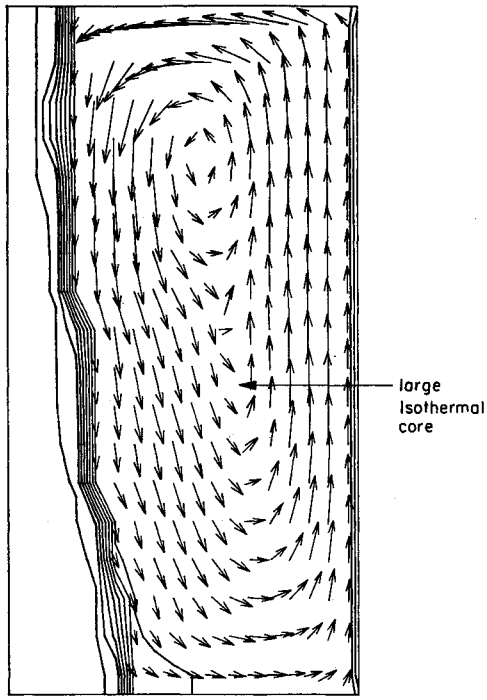

Fig. 11 Results for $Fo = 1.4$.

the fluid moves down the left side of the liquid region. However, in Fig. 12, where the solid PCM at the left boundary no longer extends entirely to the top of the domain, there is a strongly identified pair of co-rotating recirculation regions. This is believed to be the result of entrainment-like, momentum transfer driving the uppermost (expectedly) more isothermal fluid adjacent to the top left adiabatic boundary, while the lower zone is driven by the influence of the remaining cold PCM in the lower region of the left boundary through bouyancy interaction.

Clearly from the above descriptions, the phase-change melting problem is a dynamic process. As time progresses through the melting evolution significant changes occur in both the temperature field, the melt front configuration, and the velocity distribution and flow pattern. Although the interpretations given to the various figures examined are physically self-consistent, such self-consistency does not guarantee or imply accuracy of the predictions. A more quantitative evaluation, through comparison of the computed melt fraction history with the experimentally measured melt fraction history reported by Ho and Viskanta[14] and by Ho,[19] is provided in the following section.

The predicted melt fraction histories will be compared with the experimental melt fraction history reported by Ho and Viskanta[14] and by Ho.[19] Since experimental data are available only for melt fractions less than approximately 25%, the com-

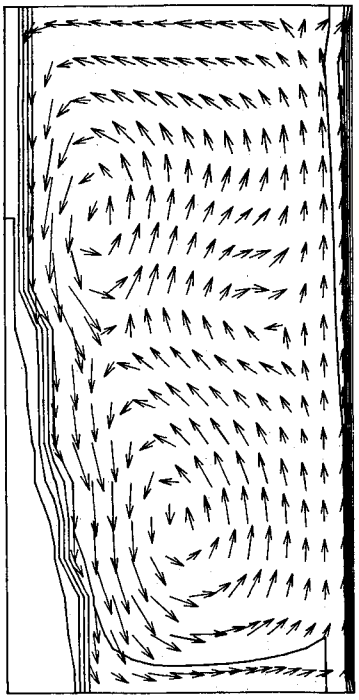

Fig. 12 Results for $Fo = 1.6$.

parisons will be restricted to this part of the evolution. Three separate computational runs were executed for this purpose. The first of these was for a 10×10 grid (8×8 interior control volumes) and the second was for a 20×20 grid (18×18 interior control volumes). The third run was performed on a 20×20 grid but the horizontal extent of the domain was reduced to one-half of the actual domain. Since the subcool is zero, the leftmost boundary does not affect the solution until the phase front reaches that boundary and for this problem this does not occur for melt fractions less than 25%. The net effect of this fluid computation, therefore, is to simulate performance on a 40×20 grid (horizontal $\times$ vertical). The computed melt fractions (computed for the half-problem) are then simply divided by two to predict full solution domain 40×20 predictions.

The results of the three computations are compared with the experimental data and with the predictions of Ho and Viskanta[14] in Fig. 13. The 10×10 grid predictions are clearly below both the data and the Ho and Viskanta predictions. This is consistent since it is expected that coarse grid computations for this problem will underpredict the melting rate. The 20×20 grid predictions are also below the experimental data and correspond clearly to the Ho and Viskanta 13×21 (horizontal $\times$ vertical), transformed liquid domain predictions. It is noted that Ho and Viskanta attributed their underpredictions to the inability of their model to account for the "flooding" that occurs over the top surface as a result of volumetric expansion of the PCM upon melting, and to the neglect of surface velocities normal to the phase front resulting from the same volumetric expansion influences.

The present 40×20 predictions are rather startling. With this increased resolution, the predictions are in excellent agreement with the experimental data. Although the computations underpredict (slightly) the data in the 0.14 to 0.16 melt fraction region, for melt fractions greater than 0.16 the computational predictions are essentially coincident with the data. At melt fractions below 0.14 this is also the case. The observations can be advanced, then, that the Ho and Viskanta postulates for their lack of agreement are not as significant as expected and, secondly, that the dependence of the prediction accuracy on grid size and spatial resolution is relatively severe.

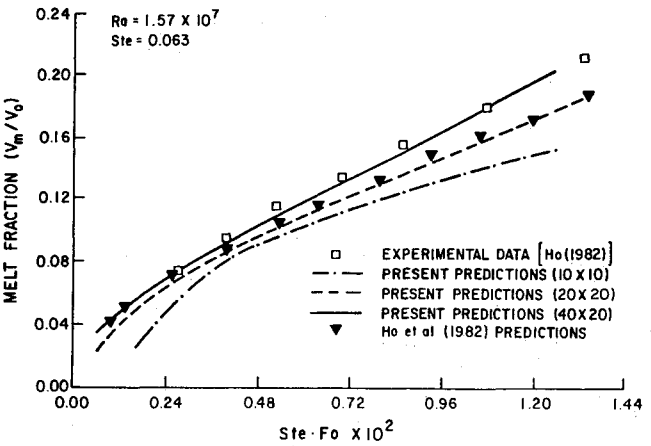

Fig. 13 Melt fraction history comparison.

Nevertheless, the extremely accurate prediction of the present fine grid (40×20) simulation provides excellent validation of the prediction computations and of the modeling of the problem physics. In view of the complexity of the phase change energy transport problem in the presence of significant free convective motion this is highly encouraging.

Computational run times for the above problem, as an entire transient evolution, remain high. However, they are significantly reduced from that reported in the work of Ho and Viskanta.[14] In their work a time per run of 50,000 CPU s (i.e., 13.9 h) was reported for a CDC 6500 installation. In comparison, the proposed procedure required 873 CPU s (i.e, 14.5 min) on an IBM 4341 installation for the 10×10 mesh size. For the 20×20 mesh size this increased to approximately 1 h of CPU time and for a true 40×40 mesh, rather than the 40×20 simulations presented here, the total execution time is approximately 4 h. While these times are indeed still large, they represent cost reductions estimated to be a factor of 30 for the same level of discretization without regard for the different installations. Such a cost reduction, however, is substantial.

Conclusions

A new numerical procedure has been presented for the computation of phase-change energy transport including the influence of free-convection motion. In the model, the conservation of mass and momentum equations are solved in addition to the conservation of thermal energy equation. An enthalpy-like model is employed in the modeling of the phase-change interface nonlinearity and the novel procedure for treating this nonlinear problem, advanced previously by Schneider and Raw[11] and Raw and Schneider[12] for diffusion dominated phase change, has been extended to the problem including free-convective motion. A coupled modified strongly implicit procedure has been employed in the solution of the coupled velocity-pressure part of the problem. The velocity of all nonliquid PCM has been assumed to be zero and is consistent with expectations for the particular problem examined.

The particular problem examined is that described by Ho and Viskanta[14] wherein a vertical isothermal boundary interacts with an initially solid PCM being insulated on all other sides and having a free surface at the top. *n*-octadecane was assumed, with $Pr_\ell = 50$, and the problem Rayleigh number was 1.57×10^7. Qualitative results have been presented which show the development of the liquid PCM. The problem was seen to be quite dynamic with several recirculation cells appearing. In addition, quantitative results have been presented in terms of the melt fraction history for the problem. Comparisons of the present predictions with the experimental results of Ho and Viskanta[14] have been presented as well as comparisons with their predictions. It was observed that the melt fraction results are relatively sensitive to the level of discretization employed

in the problem. Three levels of discretization were employed in this study. These are a 10×10 grid, a 20×20 grid, and a 40×20 grid. The present predictions for the 20×20 grid are in good agreement with the 20×13 results of Ho and Viskanta.[14] However, both of these results lie considerably below the experimental data. The lack of agreement for this grid size has been attributed by Ho and Viskanta[14] to the failure to include volumetric expansion of the PCM upon melting, in addition to possible mesh resolution inadequacy. However, the current 40×20 predictions appear to refute this conjecture. The present 40×20 results lie remarkably close to the experimental data and are significantly removed from the Ho and Viskanta[14] predictions and from the present 20×20 results.

The overall success of the present model and the present computational procedure is judged to be excellent. Not only are the predictions in excellent agreement with the experimental data but, in addition, the cost of the computational predictions is considerably lower (estimated at a factor of 30) than that incurred by the previous computations for this problem.

Acknowledgments

The author wishes to thank the Natural Sciences and Engineering Research Council of Canada and The Communications Research Centre of Canada for their financial support of this project in the form of an operating grant to G.E. Schneider and a contract to Thermofluids Research and Development, Inc., respectively. The author would also like to thank Dr. M. Zedan for performing some of the computational runs.

References

[1]Imber, M. and Huang, P.N.S., "Phase Change in a Semi-Infinite Solid With-Temperature Dependent Thermal Properties," *International Journal of Heat and Mass Transfer,* Vol. 16, Oct. 1973, pp. 1951–1954.

[2]Chung, B.T.F. and Yeh, L.T., "Freezing and Melting of Materials with Variable Properties and Arbitrary Heat Fluxes," *AIAA Journal,* Vol. 14, March 1976, 388–390.

[3]Hayashi, Y., Komori, T., and Katayana, K., "Analytical and Experiemtal Investigation of Self-Freezing," ASME Paper 75-HT-VV, ASME Winter Annual Meeting, Jan. 1975.

[4]Zien, Tse-Fon, "Analytical Study of Heat Conduction with Phase Transition," AIAA Paper 76-171, Jan. 1976.

[5]Ozisik, M.N. and Uzzell, J.C., "Exact Solution for Freezing Temperature Range," *ASME Journal of Heat Transfer,* Vol. 101, Series C, May 1979, pp. 331–334.

[6]Shamsundar, N. and Sparrow, E.M., "Analysis of Multidimensional Conduction Phase Change Via the Enthalpy Model," *ASME Journal of Heat Transfer,* Vol. 97, Aug. 1975, pp. 333–340.

[7]Ronel, J. and Baliga, B.R., "A Finite Element Method for Unsteady Heat Conduction in Materials With or Without Phase Change," ASME Paper 79-WA/HT-54, presented at the ASME Winter Annual Meeting, New York, Dec. 2–7, 1979.

[8]Baliga, R.G., personal communication, Aug. 1982.

[9]Williams, S.D. and Curry, D.M., "An Implicit Formulation for the One-Dimensional Two-Phase Multi-Interface Stefan Problem," ASME Paper 82-HT-21, presented at the 3rd AIAA/ASME Joint Fluids, Plasma, Heat Transfer and Thermophysics Conference, St. Louis, MO, June 7–11, 1982.

[10]Williams, S.D. personal communication, June 1982.

[11]Schneider, G.E. and Raw, M.J., "An Implicit Solution Procedure for Finite Difference Modeling of the Stefan Problem," AIAA Paper 83-1527, June 1983, also in *AIAA Journal,* Vol. 22, Nov. 1984, pp. 1685–1690.

[12]Raw, M.J. and Schneider, G.E., "A New Implicit Solution Procedure for Multi-Dimensional Finite Difference Modelling of the Stefan Problem," *Numerical Heat Transfer,* Vol. 8, 1985, pp. 559–572.

[13]Gadgil, A. and Govin, D., "Analysis of Two-Dimensional Melting in Rectangular Enclosures in Presence of Convection," *ASME Journal of Heat Transfer,* Vol. 106, Series C, Feb. 1984, pp. 20–26.

[14]Ho, C.-J. and Viskanta, R., "Heat Transfer During Melting from an Isothermal Vertical Wall," *ASME Journal of Heat Transfer,* Vol. 106, Series C, Feb. 1984, pp. 12-19.

[15]Patankar, S.V., *Numerical Heat Transfer and Fluid Flow,* McGraw-Hill, New York, 1980.

[16]Schneider, G.E. and Zedan, M., "A Coupled Modified Strongly Implicit Procedure for the Numerical Solution of Coupled Continuum Problems," AIAA Paper 84-1743, June 1984,

[17]Schneider, G.E. and Zedan, M., "A Modified Strongly Implicit Procedure for the Numerical Solution of Field Problems," *Numerical Heat Transfer,* Vol. 4, 1981, pp. 1-19.

[18]Schneider, G.E. and Zedan, M., "Investigation into the Stability Characteristics of Modified Strongly Implicit Procedures," ASME Paper 82-HT-23, presented at the 3rd AIAA/ASME Joint Fluids, Plasma, Thermophysics and Heat Transfer Conference, St. Louis, MO, June 7–11, 1982.

[19]Ho, C.J., "Solid-Liquid Phase Change Heat Transfer in Enclosures," Ph.D. Dissertation, Purdue University, 1982.